Field-Resolved Coherent Raman Spectroscopy of High Frequency Vibrational Resonances

ARTICLE *in* THE JOURNAL OF PHYSICAL CHEMISTRY A · OCTOBER 2006

Impact Factor: 2.69 · DOI: 10.1021/jp0645061 · Source: PubMed

3 AUTHORS, INCLUDING:

Rene A. Nome
University of Campinas
26 PUBLICATIONS **409** CITATIONS
SEE PROFILE

Norbert F. Scherer
University of Chicago
184 PUBLICATIONS **6,229** CITATIONS
SEE PROFILE

THE JOURNAL OF PHYSICAL CHEMISTRY A LETTERS

2006, *110,* 10925−10928
Published on Web 08/31/2006

Field-Resolved Coherent Raman Spectroscopy of High Frequency Vibrational Resonances

Andrew M. Moran, Rene A. Nome, and Norbert F. Scherer*

Department of Chemistry and the James Franck Institute, The University of Chicago, 5735 South Ellis Avenue, Chicago, Illinois 60637

Received: July 16, 2006; In Final Form: August 15, 2006

Electric fields of coherent Raman signals are resolved with sensitivity for high-frequency vibrational resonances utilizing a four-pulse, trapezoidal beam geometry in a diffractive optic-based interferometer. Our experiments show that the heterodyne detected signal phase is stabilized for particular terms in the third-order response function by the cancellation of inter-pulse phases. The C−H stretching modes of cyclohexane and benzene are studied under two polarization conditions. The temporal profiles of signal fields for cyclohexane exhibit a low-frequency recurrence due to the interference between the signals associated with the symmetric and asymmetric C−H stretching modes. In contrast, the electronically nonresonant polarizability response of benzene gives rise to a significant broadband signal component in addition to that associated with its C−H vibrational resonance. Time−frequency shapes of the Raman signal fields are strongly dependent on the properties of the liquid and the polarizations of the laser pulses.

Passively phase-stabilized heterodyned signal detection in transient grating and photon echo spectroscopies has recently been realized at optical frequencies by the incorporation of diffractive optics in four-wave mixing interferometers, thereby enhancing the sensitivity and information content of these techniques compared to that obtained with conventional homodyne detection.[1−8] This is more easily realized at infrared wavelengths due to significantly reduced mechanical stability requirements. Optical nonlinear spectroscopies are most useful for studying energy transfer dynamics in multilevel electronic systems,[5] whereas infrared spectroscopies provide more detailed information on molecular structure and dynamics through vibrational mode couplings.[9−13] By contrast, broadband stimulated Raman gain spectroscopy has the unique ability to resolve vibrational dynamics within a window of more than 1000 cm^{-1} with less than 100 fs time resolution in a single experiment.[14−16] Broadband optical measurements have long been undertaken[17] but pulse durations of less than 50 fs are more difficult to attain at infrared wavelengths, so the corresponding spectral range is reduced.

Nonlinear spectroscopies intrinsically possess more information at higher orders.[15,16,18−22] However, the interpretation of these experiments is complicated by interference between terms in the material response function. Dephasing-induced resonances in coherent anti-Stokes Raman spectroscopy are a good example at third order.[23−25] Therefore, electric field-resolved signal detection is essential to the development of new higher-order methods as it allows the absolute sign of the signal to be extracted and unambiguously reveals the relative magnitudes of various competing terms in the nonlinear polarization response.[7,26−29]

In this Letter, we report the new method of electric field-resolved coherent Stokes Raman spectroscopy (EFR−CSRS). The information content is demonstrated via measurements of cyclohexane and benzene in the C−H stretching region of the vibrational spectrum with a passively phase-stabilized, diffractive optic-based interferometer.[1−8] The relative polarizations of the Raman pump and Stokes pulses are varied to control the amplitudes of the vibrational bands in cyclohexane and the amount of broadband signal emission in benzene.[30] The data show that the nonresonant and vibrational resonance enhanced components of the polarization response are clearly separated with real and imaginary projections of the signals. In addition, signal fields are viewed in the spectrogram representation to analyze the signatures of various terms in the material response function on the signal pulse bandwidths, emission times and time-frequency shapes.

We emphasize that this is the first report of coherent Raman signal field resolution for resonances above ∼1000 cm^{-1} obtained with passive phase stabilization. The signal field is not completely resolved by heterodyne detection methods that provide only a particular projection of the signal field such as broadband Raman gain[14−16] and single pulse coherent anti-Stokes Raman spectroscopy (CARS).[31,32] Field-resolved CARS microscopies have been used to probe high-frequency resonances[33−35] but without the superb passive stabilization achieved with diffractive optics.[1−8]

Our experiments are performed with a home-built 1 kHz Ti:sapphire laser system[6] and the interferometer presented in Figure 1a. Briefly, the Raman pump (50 cm^{-1} bandwidth) is obtained by spectrally filtering the laser system fundamental (805 nm) in an all-reflective pulse stretcher aligned for zero dispersion. Stokes pulses (1048 nm, 40 fs) are obtained from the idler of a home-built noncollinear parametric amplifier. The Raman pump and Stokes/local oscillator (LO) pulses are crossed at an angle of 3° in a diffractive optic (DO) to generate a trapezoidal beam geometry (see Figure 1b) through the ±1 diffraction orders of each beam. The angle between the ±1 diffraction orders for the Raman pump and Stokes−LO beams are 5.0° and 6.6°,

* To whom correspondence should be addressed. E-mail: nfschere@uchicago.edu.

10.1021/jp0645061 CCC: $33.50

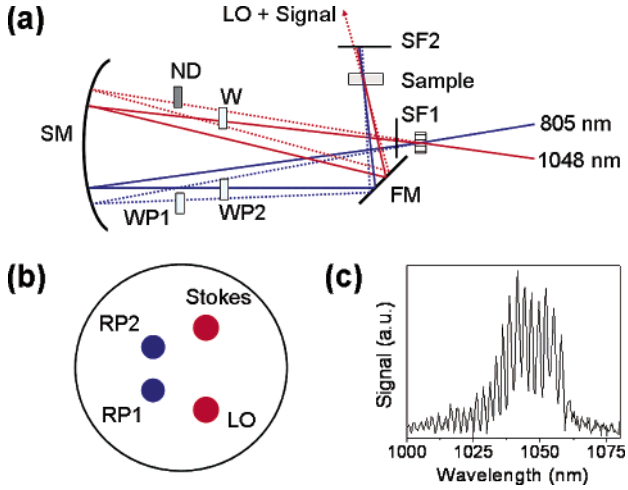

Figure 1. (a) Laser system fundamental (805 nm, 12422 cm^{-1}) and Stokes pulses (1048 nm, 9542 cm^{-1}) are focused to the same spot on a diffractive optic (DO) to generate a trapezoidal beam pattern that is directed to the sample with a 15 cm focal length spherical mirror (SM) and a flat mirror (FM). The polarizations of the Raman pump pulses are varied with the half-waveplates, WP1 and WP2. The local oscillator (LO), which is attenuated with a neutral density filter (ND), arrives to the sample 800 fs before the Stokes pulse, which is delayed with respect to the LO with a CaF_2 window (W). The spatial filters, SF1 and SF2, isolate the ±1 diffraction orders and the collinear signal+LO after the sample, respectively. (b) View of beam geometry on the SM. The RP1−RP2 (blue) and Stokes−LO (red) pulse pairs are phase-locked. Pulses represented with different colors are not phase-locked with respect to each other. (c) Interference spectrum for cyclohexane measured with parallel Raman pump and Stokes−LO polarizations.

respectively. Pulse energies at the sample are 120 nJ/pulse for each of the Raman pump beams and 2 nJ/pulse for the Stokes beam. The pulses are focused to full width half-maximum spot sizes of 80 μm in a 1 mm path length flow cell. The EFR−CSRS signal and LO are collinear after the sample and interfere in a spectrometer. The LO intensity is removed from the interference spectra by taking the difference between signals acquired at zero pulse delay (between the Raman pump and Stokes pulses) and signals obtained when the Stokes pulse arrives 5 ps before the Raman pump; the difference is taken 300 times and averaged. As shown in Figure 1c, we obtain well-resolved interference fringes over the total data acquisition time of 15 min. Data are processed by Fourier transform methods.[26,27,29]

The third-order nonlinear polarization is generally expressed as

$$P^{(3)}(\mathbf{k}_s,t) = \int_0^\infty dt_3 \int_0^\infty dt_2 \int_0^\infty dt_1\, R^{(3)}(t_3,t_2,t_1)\, E_3(\mathbf{k}_3,t-t_3) \times E_2(\mathbf{k}_2,t-t_3-t_2)\, E_1^*(\mathbf{k}_1,t-t_3-t_2-t_1) \quad (1)$$

where t_i denote the time intervals between field-matter interactions and the third-order impulse response function, $R^{(3)}(t_3,t_2,t_1)$, is a fourth rank tensor.[18] All six permutations of the electric field indices should be considered for EFR−CSRS because the peaks of the three laser pulses arrive at the sample at approximately the same time. The EFR−CSRS signal is acquired in the $\mathbf{k}_s = -\mathbf{k}_1 + \mathbf{k}_2 + \mathbf{k}_3$ phase-matched direction. Under perfect phase-matching conditions, the signal field, $E_s(\mathbf{k}_s,t)$, is related to the nonlinear polarization by[18]

$$E_s(\mathbf{k}_s,t) = \frac{i2\pi l\omega_t}{n(\omega_t)c}[P_r^{(3)}(\mathbf{k}_s,t) + P_{nr}^{(3)}(\mathbf{k}_s,t)] \quad (2)$$

where $n(\omega_t)$ is the solution's refractive index, l is the path length

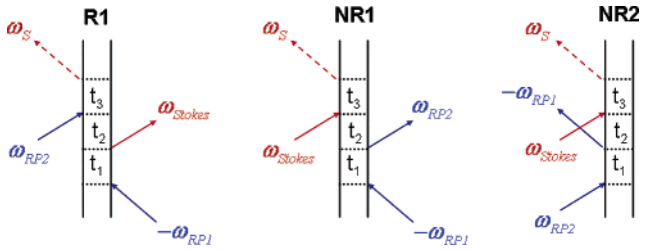

Figure 2. Double-sided Feynman diagrams for terms that contribute to the EFR−CSRS signals. The RP1−RP2 and Stokes−LO pulse pairs are represented with blue and red colors, respectively.

and c is the speed of light. $P_r^{(3)}(\mathbf{k}_s,t)$ and $P_{nr}^{(3)}(\mathbf{k}_s,t)$ represent resonant and nonresonant polarization responses, respectively.[18] The complex frequency domain signal field obtained by Fourier transformation of eq 2 with respect to t is characterized by its power spectrum, $|E_s(\omega_t)|^2$, and spectral phase, $\varphi_s(\omega_t)$: $E_s(\omega_t) = |E_s(\omega_t)| \exp[i\varphi_s(\omega_t)]$.

Equation 2 states that the EFR−CSRS signal field originates from distinct resonant and nonresonant polarization responses. The three double-sided Feynman diagrams shown in Figure 2 contribute to the EFR−CSRS signal in the rotating wave approximation.[18] $P_r^{(3)}(\mathbf{k}_s,t)$ arises from the R1 term, which has a coherence at $\omega_{RP1} - \omega_{Stokes}$ during the t_2 interval between the second and third field-matter interactions. It is therefore enhanced when this frequency matches a material resonance. This vibrational coherence decays in t_2 as the inverse line width of the respective vibrational band. In contrast, $P_{nr}^{(3)}(\mathbf{k}_s,t)$ is associated with the nonresonant broadband polarizability response of the material that originates from the NR1 and NR2 terms. The bandwidth of $P_{nr}^{(3)}(\mathbf{k}_s,t)$ is essentially the same as that of the Stokes pulse for transparent materials.

The stimulated Stokes signal frequency is given by the sum of the frequencies for each term in Figure 2; $\omega_s = \omega_{RP2} - \omega_{RP1} + \omega_{Stokes}$. The signal is phase-matched in the direction $\mathbf{k}_s = -\mathbf{k}_{RP1} + \mathbf{k}_{RP2} + \mathbf{k}_{Stokes}$ and therefore the heterodyne detected signal phase may be written as[1]

$$\varphi_{het} = [\varphi_{RP2} - \varphi_{RP1}] + [\varphi_{Stokes} - \varphi_{LO}] + \varphi_s \quad (3)$$

Bracketed terms represent "phase-locked" pulse pairs generated with the diffractive optic. These two terms possess canceling phases, and therefore the heterodyne detected signal phase, φ_{het}, is passively stabilized. This cancellation means that the Stokes and Raman pump pulses do not need to be phase-locked. This is important because these pulses traverse different paths prior to arriving at the DO; the phase of the holographic grating associated with the RP1 and Stokes pulses is not stable (i.e., the grating associated with the R1 diagram in Figure 2). However, its fluctuations are canceled by identical fluctuations in the phases of the LO and RP2 pulses. This is a unique aspect of the present experiments. Previous heterodyne-detected, diffractive optic-based four-wave mixing experiments involved polarization gratings prepared by phase-stabilized pulse-pairs.[1−8] It is worth noting that CARS signals are not passively phase-stabilized with our interferometer because the signal frequency, ω_{as}, involves the sum of the frequencies of the two Raman pump pulses (i.e., $\omega_{as} = \omega_{RP2} + \omega_{RP1} - \omega_{Stokes}$); their phases do not cancel (see eq 3).

Real and imaginary projections of the signal fields for cyclohexane and benzene are presented in Figure 3. The real part of the signal for benzene exhibits a narrow vibrational resonance enhanced component at 3065 cm^{-1}. The imaginary part of the signal consists of a relatively narrow dispersive

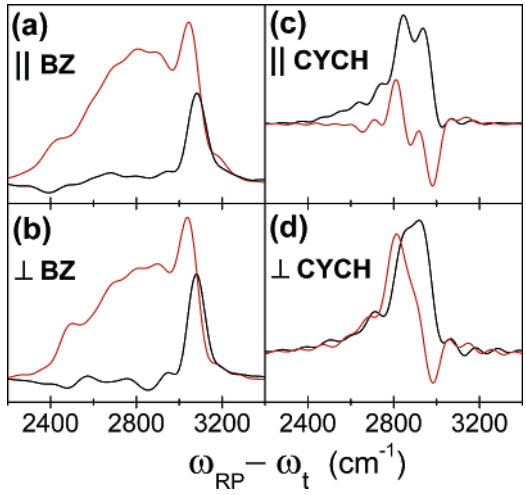

Figure 3. Real (black) and imaginary (red) projections of frequency domain EFR−CSRS signal fields obtained for (a, b) benzene and (c, d) cyclohexane. Signals acquired with parallel and perpendicular polarizations are given in panels (a−c) and (b−d), respectively. Each panel possesses an independent scale, in arbitrary units, and their magnitudes should not be compared.

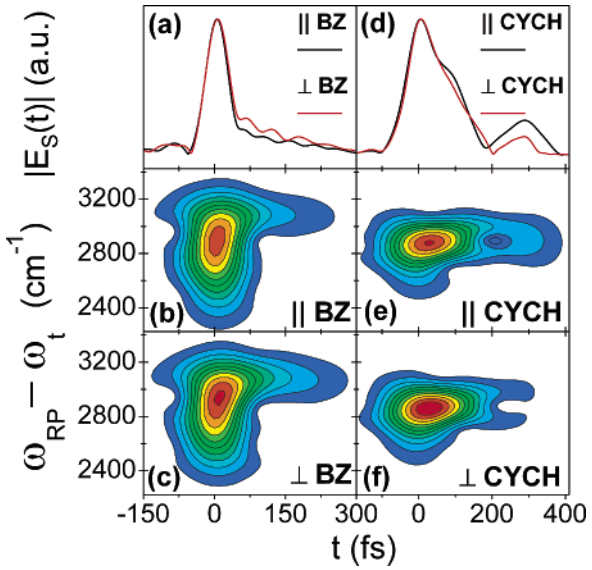

Figure 4. Absolute values of time domain signal fields (eq 2) for (a) benzene and (d) cyclohexane (right). Signal magnitudes for the two polarization conditions are normalized to their respective maximum values. Spectrograms of experimental EFR−CSRS signals are given for (b, c) benzene and (e, f) cyclohexane. Signals acquired with parallel and perpendicular polarizations are given in panels (b−e) and (c−f), respectively. The spectrograms consist of 12 equally spaced contour lines and are presented on independent scales. The polarization condition is given in the respective panel.

feature, which coincides with the vibrational resonance, superposed on top of a broader spectrum associated with $P^{(3)}_{nr}(\mathbf{k}_s,t)$. The relative strength of the broadband signal component is slightly reduced by setting the polarizations of the Raman pump pulses to be perpendicular to those of the Stokes−LO pulses. The spectra for cyclohexane show the presence of two resonances at 2850 and 2930 cm^{-1}, which correspond to the symmetric and asymmetric C−H stretching modes, respectively. In contrast to benzene, $P^{(3)}_{r}(\mathbf{k}_s,t)$ is much stronger than $P^{(3)}_{nr}(\mathbf{k}_s,t)$ for cyclohexane. The band at 2850 cm^{-1} has a smaller depolarization ratio than the band at 2930 cm^{-1} and its magnitude is reduced in the perpendicular polarization configuration.[38]

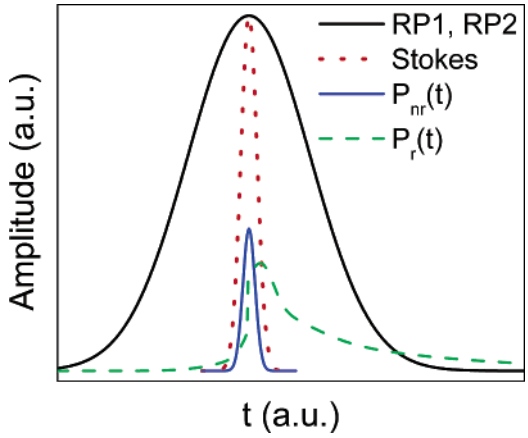

Figure 5. Schematic showing resonant (dashed green) and nonresonant (solid blue) polarization responses superposed on the Raman pump (solid black) and Stokes (dotted red) pulse envelopes. This figure assumes that $P^{(3)}_{nr}(\mathbf{k}_s,t)$ arises only from the nonresonant response of the liquid.

The top row of Figure 4 presents the time domain signal field profiles corresponding to the spectra shown in Figure 3. The signal fields for benzene consist of a short (∼40 fs) pulse associated with $P^{(3)}_{nr}(\mathbf{k}_s,t)$ emitted at $t = 0$ followed by weaker signal emission arising from $P^{(3)}_{r}(\mathbf{k}_s,t)$ with a duration of more than 200 fs. In contrast, the signal fields of cyclohexane do not exhibit the bandwidth-limited pulse structure at $t = 0$ observed for benzene. The temporal profiles for cyclohexane show a recurrence arising from interference between signals associated with the 2850 and 2930 cm^{-1} resonances. The EFR−CSRS signal spectrograms in Figure 4 are computed with

$$\Phi(\omega_t,t) = \left| \int_{-\infty}^{\infty} E_s(\tau)\, g(t-\tau)\, \exp(-i\omega_t\tau)\, d\tau \right| \qquad (4)$$

where $E_s(\tau)$ is the signal field and we take the gate function, $g(t-\tau)$, to be a Gaussian function with a full width half-maximum of 100 and 150 fs for benzene and cyclohexane, respectively. These widths are chosen to emphasize the spectral properties of the signals. Equation 4 differs from the conventional definition for the spectrogram, which is the square of $\Phi(\omega_t,t)$.[36] We do not square the right side of eq 4 to better resolve the features of the present data. The spectrograms for benzene reveal that the emission time of the resonant signal component at 3065 cm^{-1} is delayed with respect to that associated with $P^{(3)}_{nr}(\mathbf{k}_s,t)$; the nonresonant response is more dominant with parallel laser pulse polarizations. The signal spectrograms for cyclohexane exhibit a recurrence that is most prominent with the parallel polarization condition. In addition, the signal bandwidth is much narrower for cyclohexane than it is for benzene.

The data presented in Figures 3 and 4 indicate that the ratio $P^{(3)}_{r}(\mathbf{k}_s,t)/P^{(3)}_{nr}(\mathbf{k}_s,t)$ is greater for cyclohexane than for benzene. The Raman differential cross sections are similar for the C−H stretching resonances of benzene (4.45×10^{-29} cm^2 $molecule^{-1}$)[37] and cyclohexane (5.43×10^{-29} cm^2 $molecule^{-1}$), where the differential cross section for cyclohexane is computed with the depolarization ratio[38] and total cross section.[39] This analysis implies that the observed nonresonant broadband polarizability responses of the two liquids differ by approximately an order of magnitude at near-infrared (i.e., 800 nm or 12 500 cm^{-1}) frequencies. This difference cannot be rationalized with a calculation of their electronic polarizabilities using the Lorentz−Lorentz model, which requires the refractive indices and densities of the liquids as parameters. It is possible the that

strong low-frequency intermolecular mode spectrum of liquid benzene,[28,40] which possesses higher frequency content than that of cyclohexane,[41] contributes to its prominent broadband signal component through the finite pulse durations of the laser pulses. This mechanism of signal emission may also be described with the NR1 and NR2 terms of Figure 2; it yields a frequency and bandwidth similar to that of the Stokes pulse. The origin of the stronger broadband signal component observed with benzene is still under investigation.

Figure 5 illustrates the temporal properties of $P_{r}^{(3)}(\mathbf{k}_s,t)$, $P_{nr}^{(3)}(\mathbf{k}_s,t)$ and the envelopes of the Raman pump and Stokes probe pulses. As shown by the NR1 and NR2 diagrams of Figure 2, $P_{nr}^{(3)}(\mathbf{k}_s,t)$ involves two interactions with the Raman pump pulses to form a static polarization grating (i.e., no coherent evolution in t_2). The third field-matter interaction must occur within the envelope of the Stokes pulse due to the fast (i.e., quasi-instantaneous) decay of the nonresonant polarization in t_2. In contrast, the diagram R1 shows that the system interacts once with the Raman pump and once with the Stokes pulse to form a polarization grating that propagates in the $\mathbf{k}_{RP1} - \mathbf{k}_{Stokes}$ direction at a velocity of $d\omega_v$, where d is the fringe spacing ($d = 3.4\ \mu$m) and the vibrational resonance frequency is given by $\omega_v = \omega_{RP1} - \omega_{Stokes}$. The grating's phase front propagates in the direction opposite $\mathbf{k}_{Stokes} - \mathbf{k}_{RP1}$ because $\omega_{Stokes} < \omega_{RP1}$. The wavevectors, $\mathbf{k}_{RP2}$ and $\mathbf{k}_{RP1} - \mathbf{k}_{Stokes}$, differ by 10° and therefore diffraction of the RP2 pulse from this moving grating yields a signal field with the Stokes-shifted frequency $\omega_s = \omega_{RP2} - \omega_v$. The 300 fs Raman pump pulse limits the duration of the signal pulse (i.e., the spectral resolution) because it is shorter than the picosecond time scale on which the $\mathbf{k}_{RP1} - \mathbf{k}_{Stokes}$ polarization grating decays. This picture of EFR−CSRS signal generation resembles Brillouin scattering from an acoustic wave in both the signal wavevector and frequency.[42] The red-shifted (i.e., Stokes) emission frequency may be intuitively viewed as a "Doppler shift".

The time-frequency shapes of the signal fields for this novel broadband electric field-resolved Raman spectroscopy exhibit strong dependence on the laser pulse polarizations and the relative strengths of $P_{r}^{(3)}(\mathbf{k}_s,t)$ and $P_{nr}^{(3)}(\mathbf{k}_s,t)$. The three terms that contribute to the nonlinear polarization (cf. Figure 2) possess the same sign and therefore do not interfere destructively. However, this is not generally the case in third-order coherent Raman spectroscopies[23−25] and this issue poses a challenge for higher-order (nth-order) methods as the number of terms in the response function scales as 2^n. The design of these experiments requires careful analysis of the polarization response of interest to define the requirements for inter-pulse phase-locking. The present work represents an essential step in the development of higher-order spectroscopies, which generally possess interfering terms with opposite signs and therefore require signal field resolution for interpretation.

Acknowledgment. This research was supported by the National Science Foundation (CHE 0317009). R.A.N. thanks CAPES/Brazil for support through a graduate research fellowship. We thank the reviewers for helpful comments.

References and Notes

(1) Goodno, G. D.; Dadusc, G.; Miller, R. J. D. *J. Opt. Soc. Am. B* **1998**, *15*, 1791.

(2) Goodno, G. D.; Astinov, V.; Miller, R. J. D. *J. Phys. Chem. A* **1999**, *103*, 10360.

(3) Kubarych, K. J.; Milne, C. J.; Lin, S.; Astinov, V.; Miller, R. J. D. *J. Chem. Phys.* **2002**, *116*, 2016.

(4) Brixner, T.; Mancal, T.; Stiopkin, I. V.; Fleming, G. R. *J. Chem. Phys.* **2004**, *121*, 4221.

(5) Brixner, T.; Stenger, J.; Vaswani, H. M.; Cho, M.; Blankenship, R. E.; Fleming, G. R. *Nature* **2005**, *434*, 625.

(6) Moran, A. M.; Maddox, J. B.; Hong, J. W.; Kim, J.; Nome, R. A.; Bazan, G. C.; Mukamel, S.; Scherer, N. F. *J. Chem. Phys.* **2006**, *124*, 194904.

(7) Moran, A. M.; Nome, R. A.; Scherer, N. F. *J. Chem. Phys.* **2006**, *125*, 031101.

(8) Moran, A. M.; Park, S.; Scherer, N. F. *J. Phys. Chem. B.*, in press.

(9) Mukamel, S. *Annu. Rev. Phys. Chem.* **2000**, *51*, 691.

(10) Zanni, M. T.; Ge, N. H.; Kim, Y. S.; Hochstrasser, R. M. *Proc. Natl. Acad. Sci. U.S.A.* **2001**, *98*, 11265.

(11) Khalil, M.; Demirdoven, N.; Tokmakoff, A. *J. Phys. Chem. A* **2003**, *107*, 5258.

(12) Asbury, J. B.; Steinel, T.; Kwak, K.; Corcelli, S. A.; Lawrence, C. P.; Skinnter, J. L.; Fayer, M. D. *J. Chem. Phys.* **2004**, *121*, 12431.

(13) Bredenbeck, J.; Helbing, J.; Kurnita, J. R.; Wooley, G. A.; Hamm, P. *Proc. Natl. Acad. Sci. U.S.A.* **2005**, *102*, 2379.

(14) Yoshizawa, M.; Kurosawa, M. *Phys. Rev. A* **1999**, *61*, 013808.

(15) McCamant, D. W.; Kukura, P.; Yoon, S.; Mathies, R. A. *Rev. Sci. Instrum.* **2004**, *75*, 4971.

(16) Kukura, P.; McCamant, D. W.; Yoon, S.; Wandschneider, D. B.; Mathies, R. A. *Science* **2005**, *310*, 1006.

(17) Alafano, R., Ed. *The Supercontinuum Laser Source*; Springer-Verlag: New York, 1989.

(18) Mukamel, S. *Principles of Nonlinear Optical Spectroscopy*; Oxford University Press: New York, Oxford, 1995.

(19) Park, S.; Moran, A. M.; Kim, J.; Scherer, N. F. *J. Chem. Phys.* to be submitted.

(20) Underwood, D. F.; Blank, D. A. *J. Phys. Chem. A* **2005**, *109*, 3295−3306.

(21) Bredenbeck, J.; Helbing, J.; Hamm, P. *Phys. Rev. Lett.* **2005**, *95*, 083201.

(22) Hamm, P. *J. Chem. Phys.* **2006**, *124*, 124506.

(23) Bogdan, A. R.; Downer, M. W.; Bloembergen, N. *Phys. Rev. A* **1981**, *24*, 623.

(24) Andrews, J. R.; Hochstrasser, R. M. *Chem. Phys. Lett.* **1981**, *82*, 381.

(25) Rothberg, L. J.; Bloembergen, N. *Phys. Rev. A* **1984**, *30*, 820.

(26) Lepetit, L.; Chéiaux, G.; Joffre, M. *J. Opt. Soc. Am. B* **1995**, *12*, 2467.

(27) Tokunaga, E.; Terasaki, A.; Kobayashi, T. *J. Opt. Soc. Am. B* **1995**, *12*, 753.

(28) Vöhringer, P.; Scherer, N. F. *J. Phys. Chem.* **1995**, *99*, 2684.

(29) Gallagher, S. M.; Albrecht, A. W.; Hybl, J. D.; Landin, B. L.; Rajaram, B.; Jonas, D. M. *J. Opt. Soc. Am. B* **1998**, *15*, 2338.

(30) Etchepare, J.; Grillon, G.; Chambaret, J. P.; Harmoniaux, G.; Orszag, A. *Opt. Commun.* **1987**, *63*, 329.

(31) Dudovich, N.; Oron, D.; Silberberg, Y. *J. Chem. Phys.* **2003**, *118*, 9208.

(32) Lim, S. H.; Caster, A. G.; Nicolet, O.; Leone, S. R. *J. Phys. Chem. B* **2006**, *110*, 5196.

(33) Evans, C. L.; Potma, E. O.; S, X. *Opt. Lett.* **2004**, *29*, 2923.

(34) Marks, D. L.; Vinegoni, C.; Bredfeldt, J. S.; Boppart, S. A. *Appl. Phys. Lett.* **2004**, *85*, 5788.

(35) Pelletier, M. J. *Appl. Spectrosc.* **1999**, *53*, 1087.

(36) Trebino, R. *Frequency Resolved Optical Gating: The Measurement of Ultrashort Laser Pulses*; Kluwer Academic Publishers: Boston, Dordrecht, London, 2000.

(37) Schomacker, K. T.; Delaney, J. K.; Champion, P. M. *J. Chem. Phys.* **1986**, *85*, 4240.

(38) Li, B.; Myers, A. B. *J. Chem. Phys.* **1990**, *94*, 4051.

(39) Trulson, M. O.; Mathies, R. A. *J. Chem. Phys.* **1986**, *84*, 2068.

(40) McMorrow, D.; Lotshaw, W. T. *Chem. Phys. Lett.* **1993**, *201*, 369.

(41) Chang, Y. J.; Castner, E. W. J. *J. Phys. Chem.* **1996**, *100*, 3330.

(42) Boyd, R. W. *Nonlinear Optics*; Elsevier and Academic Press: London, 2002.